Peer-reviewed version available at Catalysts 2018, 8, 614; doi:10.3390/catal8120614

Communication

Highly Active Nickel-based catalyst for Hydrogen evolution in Anion Exchange Membrane Electrolysis

Alaa Y. Faid[1,*], Alejandro Oyarce Barnett[2], Frode Seland[1] and Svein Sunde [1,*]

[1] Department of Materials Science and Engineering, Norwegian University of Science and Technology, Trondheim, Norway.

[2] SINTEF Industry, New Energy Solutions Department, Trondheim, Norway.

* Correspondence: alaa.faid@ntnu.no and Svein.Sunde@ntnu.no .

Abstract: Anion exchange membrane (AEM) electrolysis is hampered by two main issues: stability and performance. Focusing on the latter, this work demonstrates a highly active NiMo cathode for hydrogen evolution in AEM electrolysis. We demonstrate an electrolyzer performance of 1 A cm^{-2} at 1.9 V (total cell voltage) with a NiMo loading of 5 mg cm^{-2} and an iridium black anode in 1 M KOH at 50 °C, that may be compared to 1.8 V for a similar cell with Pt at the cathode. The catalysts developed here will be significant in supporting the pursuit of cheap and environmentally friendly hydrogen fuel.

Keywords: Nickel; HER; Anion Exchange membrane; Electrolysis

1. Introduction

Water electrolysis utilizing a solid polymer electrolyte membrane has been widely studied.[1] Compared to traditional alkaline water electrolysis that employs porous diaphragm separators with alkaline solution electrolytes, solid polymer electrolytes provide advantages such as lower gas crossover, improved efficiency, differential pressure operation, and improved operation dynamics.[2] Two types of solid polymer electrolytes are currently being pursued: proton exchange membranes (PEMs) and anion exchange membranes (AEMs).[3] PEM water electrolysis (PEMWE) has matured considerably over the past decade, fulfilling many of the technical requirements for power-to-gas energy storage from renewables.[4,5] PEM electrolyzer technology still requires expensive catalysts based on noble metals, e.g., iridium and platinum, high cost perfluorinated polymers membranes such as Nafion.[6]

AEM water electrolysis (AEMWE) has the potential to become a cheaper alternative to PEM water electrolysis systems, for example by allowing for the use of non-precious transition metal electrocatalysts.[7] Therefore, AEM water electrolysis aims to combine the low costs of alkaline electrolysis with the high power and flexibility of PEM electrolyzers.[2] However, the water splitting performance of AEM water electrolysis is currently much lower than that of PEMWE.[8]

In general, the membrane electrode assembly (MEA) consists of a polymeric membrane with an anode and a cathode catalyst on each side of the membrane as shown in Fig 1. The catalyst can be coated on the membrane, thus forming a catalyst-coated membrane (CCM). Alternatively, catalyst ink can be coated on the porous substrate and compressed onto either side a polymer membrane forming catalyst-coated substrates (CCS).[9] In AEM water electrolysis, hydrogen gas and hydroxide ions (OH^-) produced from water reduction at the cathode while AEM exchanges (OH^-) ions to the anode.[10]

$$2H_2O \longrightarrow 2H_2 + O_2 \qquad (1)$$

Peer-reviewed version available at Catalysts 2018, 8, 614; doi:10.3390/catal8120614

The overall reaction in equation (1) requires catalytic activity, towards the oxygen evolution reaction (OER) at the anode and for the hydrogen evolution reaction (HER) at the cathode, to form the respective gases from the electrode surfaces.[11]

The overall reaction requires a theoretical free energy electrolysis voltage or thermodynamic cell voltage of 1.23 V to split water into hydrogen and oxygen at 25 °C.[12]

In practice, the cell voltage needed for efficient hydrogen generation must be higher than 1.23 V. Additional voltage is required to overcome over-voltages associated with electrode kinetics and the ohmic resistance of the electrolyte and electrolyzers components, among others.[2,13]

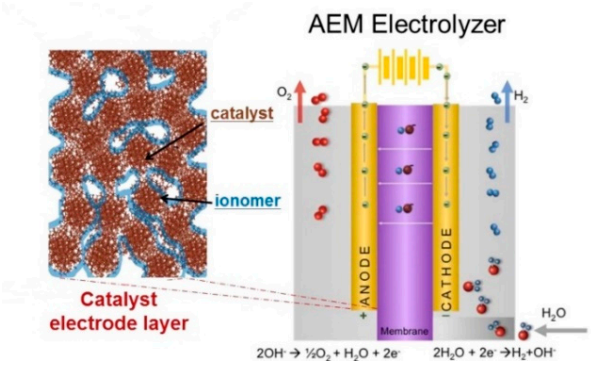

Fig 1. Catalyst electrode layer and membrane electrode assembly for AEM electrolyzer, where the catalyst is mixed with an ionomer, Reprinted from Artyushkova et al., License Number 4406040674790.[14]

Performance improvement through the development of new materials and optimization of the MEA fabrication process is of high importance. AEMs with high ionic conductivity and stability, as well as catalysts with improved activity and durability in alkaline conditions have been studied in various reports in recent years.[3,15,16] An et.al.[17] developed a mathematical model to predict the performance of AEMWE. Their results showed that an activation polarization of the hydrogen and oxygen evolution reactions is responsible for the performance reduction (voltage to achieve specific current) in AEMWE. This points to the necessity of developing high-performance MEAs through electrocatalyst and membrane optimization.[17,18]

Only a few studies address the influence of a non-precious metal catalyst cathode and hydroxide ion-conductivity in AEMWE devices. For example, Scott et al. [19,20] investigated the performance of AEMWEs using different cobalt based oxides (2.5 – 3.0 mg cm^{-2}) as the OER catalyst and Ni (2.0 mg cm^{-2}) as the HER catalyst. At a 1.9 V cell voltage, the cell achieved current densities ranging from 65 mA cm^{-2} (3.0 mg cm^{-2} of $Cu_{0.7}Co_{2.3}O_4$) to 175 mA cm^{-2} (2.5 mg cm^{-2} of Li-doped Co_3O_4). Comotti et al.[20] demonstrated the effect of HER catalyst (Ni/(CeO_2-La_2O_3)/C) loading on AEMWE performance, the current density at 1.9 V increased from 160 to 470 mA cm^{-2} as the loading varied from 0.6 to 7.4 mg cm^{-2}. Xiao et al. investigated high catalyst loadings for both the HER (NiMo 40 mg cm^{-2}) and OER (NiFe 40 mg cm^{-2}) electrodes which resulted in AEMWE performance of 570 mA cm^{-2} at 1.9 V.[21] This performance was comparable to that observed using PGM catalysts for the HER (Pt, 3.2 mg cm^{-2}), and OER (IrO_2, 2.9 mg cm^{-2}) electrodes, respectively.[1,21]

2. Results and Discussion

In this paper we show that our synthesized NiMo catalyst offers a cathode performance comparable to Pt nanoparticle catalyst in AEMWE. We also include a description of the influence of the KOH concentration on the performance of NiMo HER catalysts in a real AEMWE environment.

The NiMo catalyst was prepared by reducing an aqueous solution containing the Ni and Mo metal precursors in presence of sodium borohydride. SEM images of the amorphous catalysts are shown in Figs. S1 and S2 in electronic supplementary information (ESI†). The catalyst exhibited nanosheet-like structures. These nanosheets are loosely stacked and form sponge-like structures, leading to high specific surface areas. X-ray diffraction (XRD) indicates an amorphous nature of the

prepared catalyst as shown in Fig. S3 ESI†.[22] Raman spectra reproduced in Fig. S4 ESI†, contain peaks corresponding to the presence of one-phonon (1P) and two-photon (2P) NiO Raman modes at 570 and 1090 cm^{-1} respectively.[23] The XPS spectrum in Fig. S5 ESI† of the NiMo nanosheets displays three peaks at 230.6, 402 and 410 eV, related to Mo_{3d}, $Mo_{3p3/2}$, and $Mo_{3p1/2}$ levels of molybdenum, respectively. The NiMo nanosheets show peaks corresponding to the $Ni_{2p3/2}$ and $Ni_{2p1/2}$ levels, with binding energies 854 and 873 eV respectively, and confirms the presence of NiO. A peak with a binding energy of 187.0 eV corresponds to the of the B_{1s} level of elemental boron. [24,25]

The 25 cm^2 AEM catalyst coated membranes (CCMs) were prepared by spraying (airbrush) catalyst directly on to membranes mounted to a temperature controlled hot plate. Pt/C or NiMo supported on Vulcan x72 carbon (NiMo/X72) were used as cathode catalysts while Ir black served as the anode catalyst. Reinforced Fumatech membranes, Fumapem FAA-3-PE-30 and 10wt% Fumion FAA-3-solute-10 ionomer in NMP were utilized in the MEA preparation. The MEAs (shown in Fig. S6 in the ESI†) were assembled in a modified Baltic cell hardware between two commercially available porous Ti transport layers for water electrolysis (Beakaert). The MEAs were conditioned and exchanged to the OH form in-situ.

The morphology of the catalyst layer is best described as catalyst particles covered with ionomer and electrolyte as illustrated in Fig 1. Compositional uniformity along catalyst layers was confirmed by energy dispersive X-ray (EDX) mapping as illustrated in Fig. S7 in the ESI†; the elemental mapping shows a uniform distribution of Ni, Mo, O, and carbon. The cross-sectional interface view of the cathode MEA demonstrated in Fig. S7 (ESI†) confirmed the uniform dispersion of the catalyst along the MEA layer and its firm adherence to the membrane. SEM images (Fig. S8, ESI†) show that the distribution of catalyst is also uniform across the surface of the AEM; the SEM images revealed no voids or cracks in the catalyst layer.

The water electrolyzer setup consisted of a 5 L Teflon tank with heaters and a peristaltic pump, which was used to pump hot KOH (50 °C) through the AEMWE cell. The cells were always filled with the KOH solution during operation and were not exposed to ambient air. This eliminates some of the drawbacks associated with AEM in fuel cells, e.g., membrane degradation due to dry conditions and precipitation of carbonates. The ESI† provides more details on the preparation and testing of the AEMWE cell.

Electrochemical impedance spectroscopy (EIS) was conducted to separate the ohmic resistance from other contributions to the voltage of the AEMWE cells. Fig. 2 shows the impedance-plane plot at 0.4 A cm^{-2} for the cells with NiMo/X72 cathodes (Fig.2 a) and Pt/C cathodes (Fig.2 b) for both 0.1 and 1.0 M KOH. The impedance-plane plots appear to consist of two partly overlapping and depressed semicircles. (A high-frequency tail extending towards positive imaginary parts is considered to be due to the electronics and the experimental setup and is not considered further in this work). The low-frequency arcs are of similar size for the two catalysts, whereas the high-frequency arc has a significantly larger radius for the NiMo catalyst than for Pt.

The total ohmic resistance of the 25 cm^2 cell was determined from the high-frequency resistance (HFR), i.e., from the intercept with the real (Re) axes of the impedance-plane plot. For 1 M KOH, NiMo/X72 cell has an HFR of approximately 0.150 Ω cm^2, which is lower compared to the Pt/C based AEMWE cell (0.190 Ω cm^2) and previously reported by Cho et al.[8] This shows that despite having higher NiMo loadings resulting in thicker catalyst layers, the NiMo/X72 cell still shows excellent cell conductivity. However, a considerable increase in the HFR was observed when changing the KOH concentration to 0.1 M KOH; 0.310 Ω cm^2 for NiMo/X72 and 0.290 Ω cm^2 for Pt/C. This HFR increase at the lower KOH concentration may indicate insufficient ionic conductivity of the membrane.[26] The conductivity of the membrane is directly proportional to KOH concentration until reaches 5M KOH. Beyond this concentration, the membrane conductivity tends to decrease as KOH concentration increases.[26] The differences in the HFR between the two catalysts may be attributed to constriction resistances.[27]

Peer-reviewed version available at Catalysts 2018, 8, 614; doi:10.3390/catal8120614

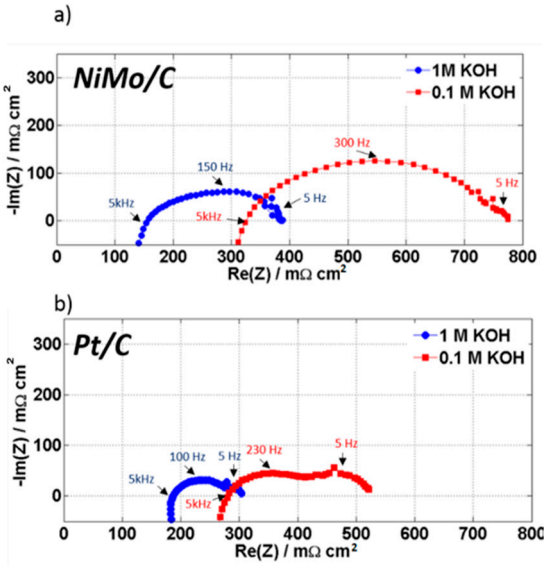

Fig 2. Electrochemical impedance taken at 0.4 A in both 1M and 0.1M KOH at 50 °C. a) 5 mg cm^{-2} NiMo loading compared to b) 1 mg cm^{-2} Pt. Cell active area: 25 cm^{-2}. Both CCMs using 3 mg cm^{-2} Ir-black.

We emphasize that apart from the cathode catalyst layers, the two cells were constructed using the same components, i.e., using the same type of bipolar plates, porous transport layers, anode catalyst layers, and membranes. Therefore, the differences in the EIS of the different cells are attributed to the cathode catalyst layer only.

The low-frequency arc at around 5 Hz (Fig. 2) being of similar magnitude in the two cases, may be attributed to mass transport[8,28,29] or the anode[30]. The much larger high-frequency arc, on the other hand, indicates significant differences in the kinetic contributions to the cell voltage from the NiMo/X72 and Pt/C cathodes. For analysis, we converted the recorded impedance data to Tafel impedance[33], i.e., the impedance multiplied with the steady-state current density at which it was obtained. For a kinetically limited process, the Tafel slope for the reaction can be found from the Tafel impedance as the diameter of the impedance arc.[30,31] Assuming that the entire impedance consists of kinetic contributions in Fig. 2, we thus estimate the Tafel slope in 1 M KOH to be 50 mV for Pt and 95 mV for NiMo (Table S1 ESI†) at 0.4 A cm^{-2}. Even if the low-frequency arc may be due to other processes than that can be ascribed to the HER at the cathode, Fig. 2, and (Fig. S9, Fig. S10, ESI†) indicates that the Tafel slope for the NiMo cell is twice that of Pt under the same process conditions. Thus, the reaction mechanism is different at NiMo cell than at Pt cell.

Fig 3 shows the polarisation curves of both iR-corrected and uncorrected voltages for the AEMWE at different KOH concentration, both for cells with cathode MEAs containing NiMo/X72 and Pt/C. For the polarisation curves that were corrected for ohmic resistance we used the following equation:

$$V_{iR} = V - (iRA) \qquad (2)$$

where V_{iR} is the potential corrected for resistance; i is the current density in units of A cm^{-2}; A is the geometric area of the AEMWEs in cm^2, and R is the area specific resistance measured by impedance and in the units of Ω cm^2. The current-voltage characteristics for the NiMo cells appear to be more curved than those for the Pt cells, both for the iR-corrected and uncorrected data. Also, the slopes of the iV-curves are larger for the cells with NiMo than those with Pt, in line with Tafel slopes from the impedance measurements.

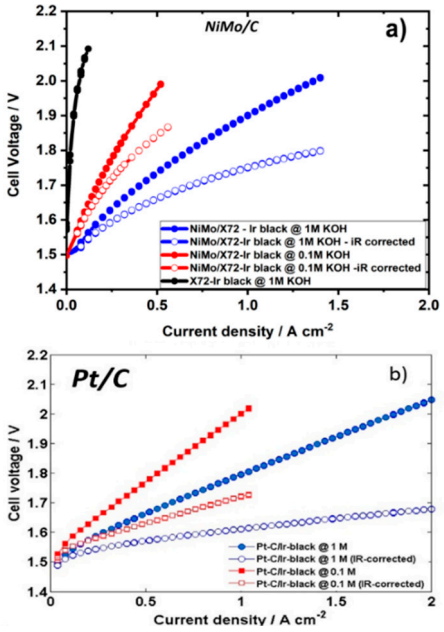

Fig 3. Polarisation curves in both 1M and 0.1M KOH at 50 °C. a) 5 mg cm^{-2} NiMo loading compared to b) 1 mg cm^{-2} Pt. Cell active area: 25 cm^{-2}. Both CCMs using 3 mg cm^{-2} Ir-black.

On the other hand, low KOH concentrations (< 1 M) does have a more adverse effect for the NiMo cell than for the Pt cell. The activity decrease in 0.1 M KOH could be related to membrane conductivity which decreases at lower KOH concentrations.[26] The different reaction mechanisms implied by the differences in Tafel impedance also suggest that the mechanisms and the reaction orders are different at the two cathodes. A contribution to the pH dependence on the overall cell performance from the cathode should therefore also be expected, as is rather clearly demonstrated in Fig. 3.

Despite higher slightly onset potentials for NiMo/X72 compared to Pt/C, the NiMo cell displays an excellent performance (Fig. 3), being comparable to that of the cell with the Pt cathode, achieving 1 A cm^{-2} at 1.9 V in 1 M KOH. The corresponding performance for the Pt cell is 1 A cm^{-2} at 1.8 V in 1 M KOH. In 0.1 M KOH, the difference was larger, the NiMo cell yielding 0.5 A cm^{-2} at 2V and the Pt cell the same current at 1.65 V. The excellent performance of 1 A cm^{-2} at 1.75 V (iR-corrected) in 1 M KOH obtained for the NiMo/X72 hydrogen catalyst outperforms all of those summarized in Table S2 ESI†. Nowadays commercial alkaline electrolyzers reach current densities up to 0.45 A cm^{-2} at a cell voltage of 1.7–2.1 V, corresponding to a theoretical hydrogen generation rate of 1.9 Nm^3 per m^3 of the cell area.[18] Therefore NiMo/X72 catalyst potentially allows for low loading transition metal loading in AEMWE operation on a commercial scale.[18,32]

3. Materials and Methods

3.1. Chemicals and materials

NiMo/X72 prepared in our lab, Commercial Pt/C (Alfa Aesar 60% on carbon support) and Ir black (Alfa Aesar 99.8% S.A> 20 m^2/g), Fumatech ionomer: Fumion FAA-3-SOLUT-10 anion exchange polymer solution N-methyl-2-pyrrolidone (NMP) solvent solution, concentration 10 wt% purchased from Fumatech BWT group, Germany.

Fumapem FAA 3 – PE membrane: Anion exchange Membrane (20-30 μm) purchased from Fumatech BWT group, Germany. Sigma Aldrich supplied reagent grade Isopropanol (IPA). All chemicals were used as received and deionized (D.I) water used was of 18.2 MΩ.cm resistivity.

NiMo Catalyst Synthesis: NiMo nanosheet prepared by reducing the aqueous mixture of Ammonium molybdate tetrahydrate $(NH_4)_6Mo_7O_{24}{\cdot}4H_2O$ and nickel nitrate hexahydrate $Ni(NO_3)_2{\cdot}6H_2O$ in the presence of sodium borohydride $NaBH_4$ to produce $Ni_{0.9}Mo_{10}$. The amorphous NiMo supported on Vulcan carbon X72 (60wt%).

3.2. Catalyst characterization

The morphology of the NiMo nanosheets was studied Using scanning electron microscopy (SEM, Carl Zeiss supra 55). NiMo nanosheets were investigated using Hitachi s-5500 FESEM, using STEM mode, NiMo dissolved in ethanol and the solution deposited on Formvar/Carbon 300 mesh, Copper grid hole size: 63µm. Structural and crystalline characteristics of the nanosheets were investigated using a Bruker D8 A25 DaVinci X-ray Diffractometer with CuKα radiation. The average wavelength of the radiation was 1.5425 Å. Raman spectroscopy was carried out with a Renishaw InVia-Reflex Spectrometer using VIS excitation at 532 nm (100mW) with spectral resolution<1 cm^{-1}. Surface electronic states and composition of NiMo nanosheets were carried out by X-ray photoelectron spectroscopy (XPS). XPS spectra were collected within an Axis Ultra DLD instrument (Kratos Analytical) equipped with a monochromatic Al X-ray source.

3.3. MEA preparation

Ink preparation: the mixing procedure includes: 1) add required amount of water (4.8 gm) and ionomer (1.92 gm) to catalyst powder then sonicate with ice for 15 minutes. 2) add IPA (4.8 gm). 3) sonicate for 10 minutes with ice. 4)Mix with an ultrasonic probe for 5 minutes with ice, amplitude = 40%. For these experiments, we keep NiMo/X72 loading 5 mg/cm^2 and Ir loading 3mg/cm^2.

Spraying MEA: 25 cm^2 MEA was done by airbrush spraying at 60 °C, a slower rate of spraying resulted in better CCM. The MEAs were fabricated using airbrush spraying. The fumatech membrane was assembled in a plastic holder that functions as a mask as well to leave only the active area open to deposition. A commercial Coltech airbrush spraying (0.35 mm nozzle) was used during the deposition. Wait 10 minutes between cathode and anode spraying.

3.3. Cell testing

For single cell tests: The MEAs were assembled in a modified Baltic cell hardware between two commercially available Ti porous transport layer for water electrolysis (Beakaert). The MEA was conditioned and exchanged to the OH form in-situ. The setup consists of 5 L Teflon tank with heaters and a peristaltic pump to pump hot KOH through the AEMWE cell. The cell was operated at 50 °C and atmospheric pressure, KOH was fed in anode and cathode sides. During cell testing, MEA with carbon only as a cathode was used to evaluate the activity of the cell without NiMo catalyst.

For electrochemical analyses, a high-current potentiostat (HCP-803, Bio-Logic) was used to control cell voltage and measure impedance. The current density was measured for repeated voltage cycles from 1.5 to 2 V. Electrochemical impedance spectroscopy (EIS) was employed to determine the cell performance–affecting resistances for different operating and electrode fabrication conditions, with the corresponding analyses performed at different current densities such as 0.1, 0.4, and 0.8 A/cm^2 in the AC frequency range of 50 kHz–200 mHz.

3.4. SEM and EDX mapping

The catalyst layers on the MEA and the cross-sectional view were examined by high-resolution scanning electron microscopy (SEM); Zeiss supra 55 was used. Samples were prepared by cutting 1.0 mm wide strips from the different MEA and fixed on aluminum holders before analysis.

4. Conclusions

In summary, we have demonstrated that the use of amorphous NiMo catalyst supported on carbon as cathode leads to AEM water electrolysis cell achieving 1 A cm^{-2} at 1.75 V (iR-corrected) in 1 M KOH supporting electrolyte. This shows that the performance of AEM water electrolysis may be achieved at levels (especially on a cost vs. current basis) of significant commercial interest.

Supplementary Materials: The following are available online, Fig S1: a) SEM image of NiMo nanosheets, Fig S2 a) Inverted dark field STEM NiMo nanosheets b) NiMo supported in Vulcan x72 prepared by chemical reduction, Fig S3: X-ray diffraction pattern of NiMo nanosheets, Fig S4: Raman spectrum of NiMo nanosheets,

Fig S5: XPS spectrum of NiMo nanosheets, Fig S6:photograph of an individual MEA, Fig S7: a) SEM image of MEA cross-section, b) EDX mapping of MEA prepared by airbrush spraying, and individual elemental mapping for Ni, Mo, O, and C respectively, Fig S8: a) SEM image of NiMo/x72 cathode surface in MEA, b) SEM image of Ir anode surface in MEA prepared by airbrush spraying, Fig S9: Tafel analysis of a) NiMo/X72 cell and b) Pt/C cell in 1 and 0.1 M KOH, Fig S10: Tafel impedance analysis of a) and b) NiMo/X72 cell in 0.1 M and 1 M KOH respectively, c) and d) Pt/C cell in 0.1 and 1 M KOH respectively, Table S1 Tafel impedance of NiMo/X72 cell and Pt/C cell in 0.1 and 1M KOH at different current density, Table S2 Review of AEM water electrolysis performance and development.

Author Contributions: Synthesis, electrochemical measurements, SEM, STEM, XRD, Raman, XPS data analysis, writing and editing, Alaa Y. Faid; In-situ electrolysis testing, Funding acquisition, supervision, review and editing, Alejandro Barnett; Supervision, funding acquisition, review and editing, Frode Seland; Funding acquisition, supervision, review and editing, Svein Sunde.

Acknowledgments: Financially support from the Research Council of Norway, ENERGIX, HAPEEL, project number 90218402, is greatly acknowledged. The Research Council of Norway is acknowledged for the support to the Norwegian Micro- and Nano-Fabrication Facility, NorFab, project number 245963/F50.

Conflicts of Interest: "There are no conflicts to declare."

References

1. Vincent, I., Kruger, A. & Bessarabov, D. Development of efficient membrane electrode assembly for low cost hydrogen production by anion exchange membrane electrolysis. *Int. J. Hydrogen Energy* **42,** 10752–10761 (2017).
2. Leng, Y. *et al.* Solid-state water electrolysis with an alkaline membrane. *J. Am. Chem. Soc.* **134,** 9054–9057 (2012).
3. Varcoe, J. R. *et al.* Anion-exchange membranes in electrochemical energy systems. *Energy Environ. Sci.* **7,** 3135–3191 (2014).
4. Sapountzi, F. M., Gracia, J. M., Weststrate, C. J. (Kees-J., Fredriksson, H. O. A. & Niemantsverdriet, J. W. (Hans). Electrocatalysts for the generation of hydrogen, oxygen and synthesis gas. *Prog. Energy Combust. Sci.* **58,** 1–35 (2017).
5. Grond, L., Schulze, P. & Holstein, J. Systems Analyses Power to Gas. *DNV Kema* **GCS 13.R.2,** 1–70 (2013).
6. Kuckshinrichs, W., Ketelaer, T. & Koj, J. C. Economic Analysis of Improved Alkaline Water Electrolysis. *Front. Energy Res.* **5,** (2017).
7. Gong, M., Wang, D. Y., Chen, C. C., Hwang, B. J. & Dai, H. A mini review on nickel-based electrocatalysts for alkaline hydrogen evolution reaction. *Nano Res.* **9,** 28–46 (2016).
8. Kyung, M. *et al.* Factors in electrode fabrication for performance enhancement of anion exchange membrane water electrolysis. *J. Power Sources* **347,** 283–290 (2017).
9. Phillips, R. & Dunnill, C. W. Zero gap alkaline electrolysis cell design for renewable energy storage as hydrogen gas. *RSC Adv.* **6,** 100643–100651 (2016).
10. Xiang, C., Papadantonakis, K. M. & Lewis, N. S. Principles and implementations of electrolysis systems for water splitting. *Mater. Horiz.* **3,** 169–173 (2016).
11. Eftekhari, A. Electrocatalysts for hydrogen evolution reaction. *Int. J. Hydrog. Energy* **42,** 11053–11077 (2017).
12. Li, X., Hao, X., Abudula, A. & Guan, G. Nanostructured catalysts for electrochemical water splitting: current state and prospects. *J. Mater. Chem. A* **4,** 11973–12000 (2016).
13. Bladergroen, B., Su, H., Pasupathi, S. & Linkov, V. Overview of Membrane Electrode Assembly Preparation Methods for Solid Polymer Electrolyte Electrolyzer. in *Electrolysis* (Intech, 2012). doi:10.5772/52947

14. Artyushkova, K. *et al.* Application of X-ray photoelectron spectroscopy to studies of electrodes in fuel cells and electrolyzers. *J. Electron Spectros. Relat. Phenom.* (2017). doi:10.1016/j.elspec.2017.12.006
15. Cho, M. K. *et al.* Alkaline anion exchange membrane water electrolysis: Effects of electrolyte feed method and electrode binder content. *J. Power Sources* **382,** 22–29 (2018).
16. Sassin, M. B., Garsany, Y., Gould, B. D. & Swider-Lyons, K. E. Fabrication Method for Laboratory-Scale High-Performance Membrane Electrode Assemblies for Fuel Cells. *Anal. Chem.* **89,** 511–518 (2017).
17. An, L., Zhao, T. S., Chai, Z. H., Tan, P. & Zeng, L. Mathematical modeling of an anion-exchange membrane water electrolyzer for hydrogen production. *Int. J. Hydrog. Energy* **39,** 19869–19876 (2014).
18. Buttler, A. & Spliethoff, H. Current status of water electrolysis for energy storage, grid balancing and sector coupling via power-to-gas and power-to-liquids: A review. *Renew. Sustain. Energy Rev.* **82,** 2440–2454 (2018).
19. Wu, X. & Scott, K. A non-precious metal bifunctional oxygen electrode for alkaline anion exchange membrane cells. *J. Power Sources* **206,** 14–19 (2012).
20. Pavel, C. C. *et al.* Highly efficient platinum group metal free based membrane-electrode assembly for anion exchange membrane water electrolysis. *Angew. Chemie - Int. Ed.* **53,** 1378–1381 (2014).
21. Xiao, L. *et al.* First implementation of alkaline polymer electrolyte water electrolysis working only with pure water. *Energy Environ. Sci.* **5,** 7869–7871 (2012).
22. Nie, M., Zou, Y. C., Huang, Y. M. & Wang, J. Q. Ni-Fe-B catalysts for NaBH4hydrolysis. *Int. J. Hydrog. Energy* **37,** 1568–1576 (2012).
23. Mironova-Ulmane, N. *et al.* Raman scattering in nanosized nickel oxide NiO. *J. Phys. Conf. Ser.* **93,** (2007).
24. Gupta, S. *et al.* Co-Mo-B Nanoparticles as a non-precious and efficient Bifunctional Electrocatalyst for Hydrogen and Oxygen Evolution. *Electrochim. Acta* **232,** 64–71 (2017).
25. Gupta, S. *et al.* Co-Ni-B nanocatalyst for efficient hydrogen evolution reaction in wide pH range. *Appl. Catal. B Environ.* **192,** 126–133 (2016).
26. Kraglund, M. R. *et al.* Zero-Gap Alkaline Water Electrolysis Using Ion-Solvating Polymer Electrolyte Membranes at Reduced KOH Concentrations. *J. Electrochem. Soc.* **163,** F3125–F3131 (2016).
27. Fleig, J. The Influence of Current Constriction on the Impedance of Polarizable Electrodes. *J. Electrochem. Soc.* **144,** L302 (1997).
28. Dedigama, I. *et al.* In situ diagnostic techniques for characterisation of polymer electrolyte membrane water electrolysers - Flow visualisation and electrochemical impedance spectroscopy. *Int. J. Hydrogen Energy* **39,** 4468–4482 (2014).
29. Sun, S., Shao, Z., Yu, H., Li, G. & Yi, B. Investigations on degradation of the long-term proton exchange membrane water electrolysis stack. *J. Power Sources* **267,** 515–520 (2014).
30. Jaouen, F., Lindbergh, G. & Wiezell, K. Transient Techniques for Investigating Mass-Transport Limitations in Gas Diffusion Electrodes. *J. Electrochem. Soc.* **150,** A1711 (2003).
31. Darab, M., Barnett, A. O., Lindbergh, G., Thomassen, M. S. & Sunde, S. The Influence of Catalyst Layer Thickness on the Performance and Degradation of PEM Fuel Cell Cathodes with Constant Catalyst Loading. *Electrochim. Acta* **232,** 505–516 (2017).
32. Vincent, I. & Bessarabov, D. Low cost hydrogen production by anion exchange membrane electrolysis: A review. *Renew. Sustain. Energy Rev.* **81,** 1690–1704 (2018).